doi: 10.56761/EFRE2022.S1-P-049002

Auxiliary orbitron glow discharge of a wide aperture electron accelerator based on ion-electron emission

A.A. Grishkov[*], *M.S. Vorobyov, S.Yu. Doroshkevich, V.A. Shklyaev*

Institute of High Current Electronics SB RAS, Tomsk, Russia
[*]*grishkov@to.hcei.tsc.ru*

Abstract. In this paper, the region of an auxiliary orbitronic glow discharge in an electron accelerator based on a non-self-sustained high-voltage glow discharge is investigated. The paper presents an analytical approach and the results of test modeling of an orbitron glow discharge with a hollow cathode, which plays the role of an auxiliary discharge for plasma generation with subsequent extraction of ions from it into the main high-voltage gap. In this glow discharge, the anode is two tungsten wires, and the cathode is the inner walls of the chamber, bounded by the anode and support grids of the accelerator. In the model, these regions are considered as separate and independent, but which are connected by a layer of conducting plasma that matches the boundary conditions. A model based on the representation of an auxiliary glow discharge in the form of matched electron and ion diodes makes it possible to estimate the range of possible voltages for each of the near-electrode layers and to determine the plasma potential.

Keywords: orbitron glow discharge, electron accelerator based on ion-electron emission, non-self-sustained high-voltage glow discharge, pulse mode, Child-Langmuir conditions, computer simulation.

1. Introduction

At present, low-energy electron accelerators based on plasma emitters with the extraction of a large-section electron beam into the atmosphere are used in various fields of science and technology: in laboratory research, in medicine, in the creation of new materials, and other problems [1–8]. In the present work, one of the elements of this type of accelerators is investigated, namely, the region of the auxiliary discharge of an electron accelerator based on a non-self-sustained high-voltage glow discharge. The electron beam in the accelerator is generated by ion-electron emission during the bombardment of the cathode by ions extracted from the plasma of this auxiliary discharge.

Due to the development of the modern element base, it has become possible to create discharge power supplies with the transition from the stationary mode of generating an auxiliary discharge to a repetitively pulsed mode with a pulse repetition rate at the level of a few to tens of kHz [9]. Unfortunately, in the pulsed mode, the already complex system of dependences of the parameters of ion and electron beams on the external control parameters of the discharge becomes even more complicated. This is due to the fact that the ignition of the auxiliary discharge, the extraction of ions, and the output of the electron beam into the atmosphere occur under the conditions of relaxation of the plasma that was generated by the previous pulse. This has an ambiguous effect on the stability of the configuration of the ion-electron optical system. In addition, diagnostics is complicated under these conditions, since in addition to the usual engineering tasks associated with measuring the parameters of the emission plasma, there is also a synchronization problem. Deviation from the optimal parameters leads to the fact that the electrons emitted from the surface of the high-voltage cathode are not emitted into the atmosphere, but remain as energy losses on the anode or output grid of the output foil window.

At present, the transition to a pulsed mode with a pulse repetition rate of a few to tens of kilohertz kHz has made it possible to increase the current output coefficient from 0.25 in the continuous mode to more than 0.5 in the repetitively pulsed mode of operation [10]. The current output coefficient is equal to the ratio of the beam current in the atmosphere to the current in the accelerating gap. The transition to the pulsed mode made it possible to move into the region of record-breaking parameters in terms of the discharge current, beam current, and current extraction coefficient for this type of accelerator at relatively low average values of the auxiliary discharge

current and the generated electron beam. However, the problem of stable production of beams with high power density and average power under conditions of satisfactory beam homogeneity is still relevant.

In this paper, we study one of the structural units of this type of accelerators, namely, the region of an auxiliary glow discharge of an orbitron type with a hollow cathode, and the aim of the work is to develop a model that will allow predicting data on the configuration of an ion-electron optical system depending on the external parameters of the auxiliary discharge. The creation of such a model is necessary to select the optimal modes of generation of the emission plasma, which differ in the efficiency of the selection of ions from it, their acceleration, and the corresponding efficient extraction of the electron beam into the atmosphere. The knowledge of the plasma potential, its other parameters, and emission processes will make it possible to develop rules and recommendations for improving the stability of the accelerator, which consists in reducing the number of electrical breakdowns in the high-voltage accelerating gap, which will contribute to high stability of the operational parameters and output characteristics of the accelerator.

2. Experimental setup

The design of the accelerator (Fig.1) includes two main areas: the area of generation of an auxiliary glow discharge of the orbitron type for creating an anode plasma and the area of combustion of the main non-self-sustaining high-voltage glow discharge. In this paper, we will focus on the auxiliary discharge. The auxiliary discharge is generated in a cylindrical chamber with a diameter of 1070 mm and a height of 145 mm. The role of the auxiliary discharge is performed by an independent glow discharge of the orbitron type with a hollow cathode, in which the anode is two tungsten wires 850 mm long and a diameter 0.3 mm, and the cathode is the walls of the vacuum chamber, bounded by two grids – anode and output, perforated with coaxial holes with parameters 8 ×100 mm, with rounded edges. In this case, in the emitter electrode system, two identical parallel wires are located along the long sides of the anode grid “in the shadow” of the generated electron beam. The working gas (helium) is injected into the region of the auxiliary discharge between the wire anodes. The auxiliary discharge is generated using a current source with stabilization of the average value, which is capable of operating in continuous and repetitively pulsed modes with a frequency of 1–100 kHz. Typical oscillograms of the current and voltage of the auxiliary discharge are shown in Fig.2. Auxiliary discharge voltage 400–800 V, discharge current 30–150 mA, working gas pressure $(7–40)\cdot 10^{-3}$ Torr. On the given oscillogram, the average auxiliary discharge current is 50 mA, the discharge generation frequency is 5 kHz, and the duty cycle 80%. The installation elements, operating ranges of experimental measurements, and diagnostic features are described in more detail in [10–12].

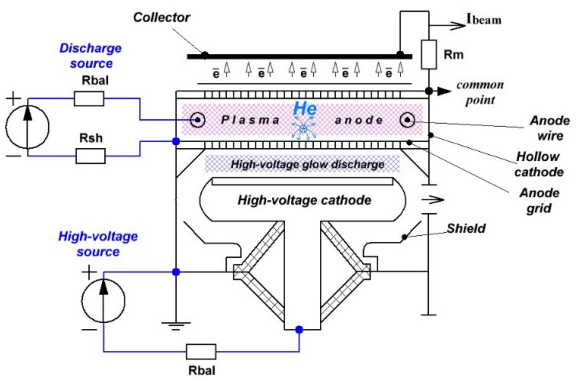

Fig.1. Design of wide-aperture electron accelerator based on ion-electron emission in repetitively pulsed mode.

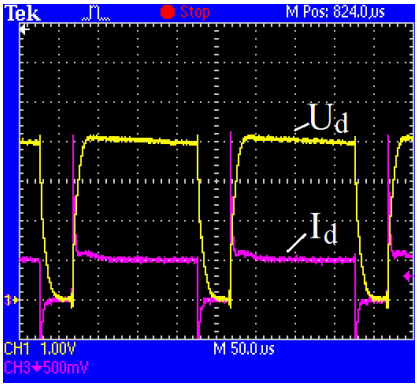

Fig.2. Oscillogram of the current and voltage of the glow discharge. CH1 – discharge voltage (140 V/div); CH2 – discharge current (50 mA/div).

2. Theory

In the considered electrode system of the accelerator, an independent glow discharge is implemented, which plays the role of an auxiliary one and is used to generate plasma with subsequent extraction of ions from it into the main high-voltage gap. Let us represent the auxiliary discharge region as two separate and independent regions, the anode and the cathode, which are connected by a layer of conductive plasma that matches the boundary conditions. A photograph of the glow of the anode plasma, as well as the proposed schemes of the cathode and anode regions of the auxiliary discharge are shown in Fig.3.

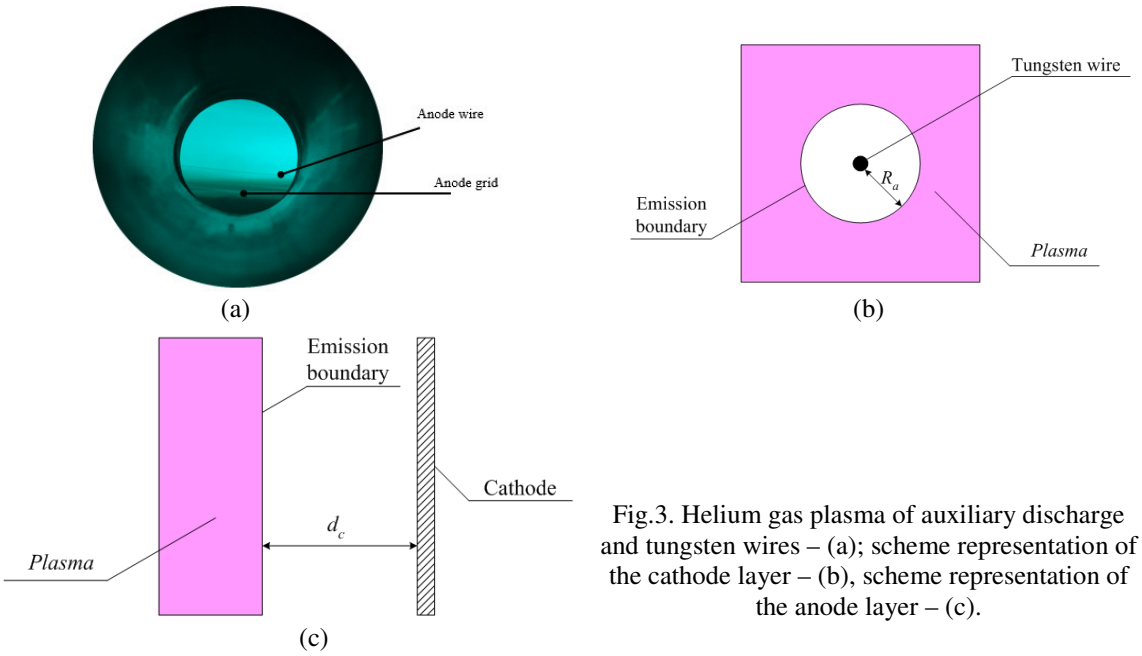

Fig.3. Helium gas plasma of auxiliary discharge and tungsten wires – (a); scheme representation of the cathode layer – (b), scheme representation of the anode layer – (c).

The anode layer is represented by two parallel identical wires. We assume that the electron current is uniformly distributed over the wires and there are no emission processes at the anode. Consequently, the total current to the anode is provided by electrons, and we can simulate this part of the discharge by a cylindrical electron diode, in which the Child-Langmuir current flows from the plasma to the wires. Of course, this is a rather rough assumption, since there are experimental data on the non-uniform distribution of plasma inside the chamber (the concentration is higher in the central part [11]). However, the difference in concentration between the region near the axis of the system and at the periphery is not so great, and, if necessary, can be described in terms of correction factors. In this regard, we believe that it is quite justified to use such a simple approximation at this stage.

The cathode for the auxiliary glow discharge is the walls of the chamber (a cylinder limited by two gratings). It is reasonable to consider this part of the discharge as a flat ion diode, since in the normal mode of operation of the generator one tends to conditions under which there are no cathode spots. Consequently, in these modes there are no significant electron emission processes at the cathode. Similarly, we will assume that the total current to the cathode of the auxiliary discharge is transferred only by ions and there is no even partial compensation of the space char. This is also a rough approximation, since we must postulate that the ion current density on the side surface of the chamber and the flat part does not depend on how far they are from the center of the chamber. This is hardly applicable for the entire range of operating parameters, since cathode spots are still observed in a number of regimes. In this case, this diode will also need to be considered from the

standpoint of the presence of a secondary ion-electron emission coefficient on the chamber walls, which will entail a change in the current-voltage characteristic of this layer. But in the framework of this work, we restrict ourselves to a simple approximation.

To describe an ion diode, we use the well-known relation for the Child-Langmuir current [13, 14], in which the mass of particles is equal to the mass of helium molecules:

$$I_c = \frac{4}{9}\varepsilon_0\sqrt{\frac{2e}{M_i}}\frac{S_c}{d_c^2}U_c^{\frac{3}{2}}, \tag{1}$$

where S_c is the surface area of the hollow cathode, d_c is the width of the cathode layer, U_c is the voltage in the cathode layer, e is the electron charge, M_i is the ion mass, and ε_0 – is the electric constant. Accordingly, the impedance of the cathode layer:

$$Z_c = \frac{U_c}{\frac{4}{9}\varepsilon_0\sqrt{\frac{2e}{M_i}}\frac{S_c}{d_c^2}U_c^{\frac{3}{2}}}. \tag{2}$$

We can estimate the characteristic impedance values for layers based on the size of the chamber. Substituting the values, we find that in the operating range of the discharge parameters, the impedance of the layers is in the range of units of kOhm.

The description of the anode layer is more complicated. First, it is a cylindrical diode for which there is no rigorous analytical solution. According to [14, 15], the calculation of the current limited by the space charge for this case can be represented by the following dependence:

$$I_a = \frac{8\pi}{9}\varepsilon_0\sqrt{\frac{2e}{m_e}}\frac{l_a}{\beta^2 R_a}U_a^{\frac{3}{2}}, \tag{3}$$

where l_a is the rod length, R_a is the anode radius, U_a is the voltage in the anode layer, β is a transcendental function depending on the ratio of the anode and cathode radii, which can be represented as a convergent infinite series or use the tabular value of this function [15]. In this case, we will be interested in the coefficient ($-\beta^2$), which corresponds to emission from an electrode of a larger diameter. Impedance of the anode layer:

$$Z_a = \frac{U_a}{\frac{8\pi}{9}\varepsilon_0\sqrt{\frac{2e}{m_e}}\frac{l_a}{\beta^2 R_a}U_a^{\frac{3}{2}}}. \tag{4}$$

However, the convergence of the series at large ratios of the emitter radius to the collector radius is insufficient. This is exactly our case, since the collector is a thin wire. In this case, approximate analytical expressions are proposed [15, 16].

$$\beta^2 = 4.6712\left(\frac{r_0}{r}\right)\left[\log_{10}\left(\frac{r_0}{r}\right) - \log_{10}(\sqrt{2})\right]^{\frac{3}{2}} \tag{5}$$

A set of isolines with the same voltage value on the cathode and anode layers is shown in Fig.4. This type of isolines is determined by the fact that the impedance is proportional to the square of the layer width and inversely proportional to the voltage.

Let's analyze Fig.4 and make some important remarks. First, the anode layer is thinner than the cathode one (because the distribution of the electric field in it is more non-uniform). Secondly, its

impedance has a much steeper increase from the width of the anode layer. Fig.4 also shows the dependences of the impedance on the voltage for isolines with the same value of the total current.

Let us make an estimate for the following parameters of the auxiliary discharge: discharge voltage $U_d \approx 400$ V, discharge current $I_d = 50$ mA. Consequently, $Z_d = 8$ kOhm (discharge parameters for which probe measurements were made with determination of the plasma potential) [10–12].

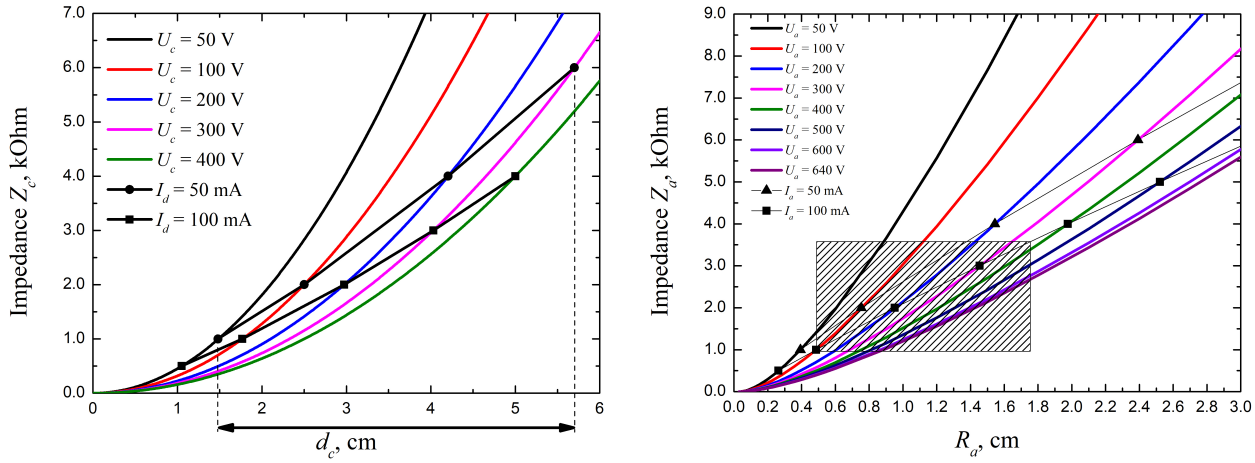

Fig.4. Dependence of the impedance on the voltage in the layer and the distance for the cathode and anode layers. The curves with symbols are isolines for the same diode currents of 50 mA and 100 mA. The shaded zone is the area of estimation of parameters for voltages.

2.1. Analysis of the parameters of the cathode and anode layers

The width of the cathode layer in Fig.4a is limited to 6 cm. This is because the cathode layer cannot be wider. Since in this case the cathode layers on different sides of the chamber will be larger than its transverse dimension. In addition, not the transverse size of the chamber, but the distance from the edge of the anode grid to the tungsten wires can be used for evaluation. The parameters that close this range (arrow in Fig.4a) allow us to conclude that the voltage in the cathode layer should be less than 300 V (isoline 50 mA, from black to magenta curve), and the layer impedance, respectively, $Z_c \leq 6$ kOhm.

Having determined Z_c, we find the anode layer impedance in the range 2 kOhm $\leq Z_a \leq 8$ kOhm. Therefore, from the graph in Fig.4b we can determine the range of allowable voltages in the anode layer. It is 100 V $\leq U_a \leq 400$ V (shaded area in the figure). What other areas can we exclude? It is logical to remove very low voltages in the cathode layer. From the trajectory analysis we carried out for this accelerator, we determined that at low voltages, most of the ion beam is deposited onto the anode grid. From the simulation of ion beam ray tracing [17], we found that ion trajectories are significantly distorted when the plasma boundary is curved. This occurs at voltages in the layer are less then ≤50 V.

Thus, using this model, we can estimate the voltage in the anode layer in the range of 100 V $\leq U_a \leq 350$ V and for the cathode layer 50 V $\leq U_c \leq 300$ V. From experimental measurements [10–12] for a diode current value of about 50 mA, the potential plasma relative to the cathode was $U_p \approx$ 180–220 V. This is in our estimate, the values lie close to the upper limit for the cathode layer and the lower limit for the anode layer.

Thus, the model based on the representation of the auxiliary glow discharge as matched electron and ion diodes makes it possible to estimate the range of possible voltages for each of the near-electrode layers. For the minimum current value of the auxiliary glow discharge, the voltage

interval is 250 V. We can also determine the threshold value for the ignition current of the auxiliary discharge. For example, according to the model, it turns out that for $U_d \approx 400$ V and $I_d < 25$ mA we have no solution, since the width of the layers becomes comparable to or larger than the dimensions of the chamber. This is in good agreement with the experimental results, since the discharge is not stably ignited for lower currents.

3. Simulation

Unfortunately, the complex geometry of the accelerator does not allow direct modeling of the auxiliary discharge region. Since such a problem must be solved in a full 3D formulation, and at the moment there is no such software that would allow modeling all elements of the accelerator in full scale. And even if such software were available, the processing power requirements would be excessive. Therefore, from the point of view of modeling, it is logical to divide this problem into its constituent parts and study them separately by "sewing" solutions at the boundaries.

We tried to simulate an auxiliary discharge using a beam model using the open source PIC code xoopic and its commercial version, the OOPIC Pro code [18]. The idea was that in the discharge between the cathode and anode layers, the voltages would be distributed self-consistently, based on the magnitude of the discharge current and plasma parameters (plasma density, electron and ion temperatures). We can implement similar conditions in the simulation when currents are injected, which are generated by oppositely charged particles. In this case, the voltage is distributed in proportion to the discharge current, the particle mass factor and the geometric factor.

Consider a flat diode to which a static constant voltage U_0 is applied, which is comparable in order of magnitude with the voltage in the auxiliary glow discharge. At the center of this diode in a thin layer, we set the following emission condition. Let electrons and positrons be created in this diode in its central part at a constant rate. Let the mass of these positrons be twice as large as the mass of electrons. In a real experiment, the particle masses differ significantly, but this is compensated by the inverse ratio of the cathode and anode areas. For now, for simplicity, we will assume that electrons and positrons appear with a uniform concentration distribution profile and with a thermal initial velocity in a thin layer at the geometric center of the diode.

Let us denote the rate of this generation as $\Psi(t)$, the dimension of which will be [$C \cdot m^{-3} \cdot c^{-1}$]. In real conditions, such a situation will correspond to external ionization of the gap, such that a direct current is generated in a given volume.

Fig.5 shows the results of test simulation for the flat and cylindrical cases for a unit volume, as well as the distribution of the potential and the distribution of macro-particles of both types in the diode.

Calculations show that with the injection of a current greater than the Child-Langmuir current (for both types of particles for a half gap and realized voltage), three characteristic layers formed in the system. A layer of "beam plasma" has formed in the central part of the diode – an extended region in space with an almost completely compensated space charge, which will expand until its boundaries reach a certain critical position. In this position, the Child-Langmuir current will be emitted from the boundary of the region, which corresponds to the value of the injected current specified by us through the generation function $\Psi(t)$. The total current, for example, for a flat case will be equal to:

$$j = \Delta x \cdot \Delta y \cdot \Psi\left(t\right),$$

that is the size of the injection area along the x-axis and y-axis, multiplied by the rate of charge injection. In the framework of this work, we do not yet focus on the average energy of electrons and positrons inside this "beam plasma". With the available processing power and the ability to change

the particle enlargement factor, it is enough to ensure that the temperature of electrons and positrons is significantly lower than the minimum realizable voltage in the layers. In our conditions, the code was used in two geometry configurations: flat *xy* and cylindrical *rz*. The computational grid consisted of up to 200×200 cells, the time step was 10^{-11}–10^{-15} s, and the number of macroparticles was up to 10^7 pcs. Under these conditions, the electron temperature did not exceed 1 eV. At the same time, no special numerical methods were used to stabilize the calculation or numerical cooling of this "plasma", such as numerical filtering, limiting the particle energy, etc.

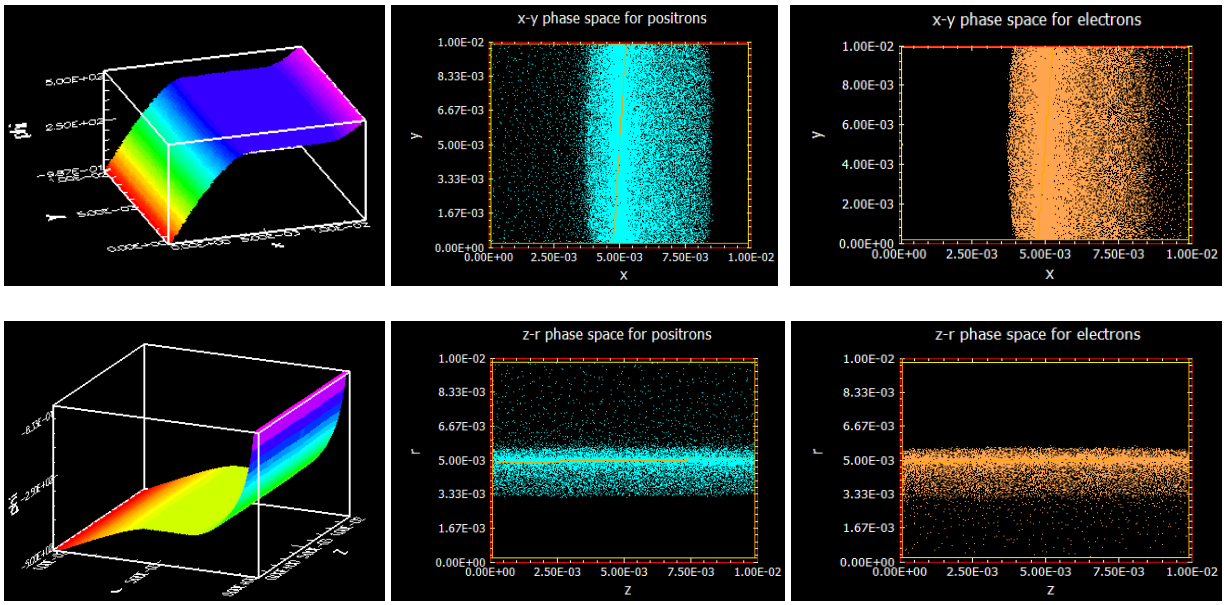

Fig.5. Distributed beam plasma for a planar and cylindrical diode. Distribution of potential, electron and ion particle plot in the gap. Simulation for electrons and positrons with $m_p = 2m_e$.

In this way we can describe the behavior of the layers, provided that we know the initial position of the emission region. In our case, the accelerator has central symmetry, so the choice of the central part of the diode is justified. However, when matching diodes, we can place the boundary condition for particle generation in different parts of the diode.

Fig.6 shows the dependences of the plasma boundary position and voltage in the cathode and anode layers obtained using the OOPIC Pro simulation for a flat *xy*-geometry. For this series of calculations, simulations were carried out in a unit volume, the masses of electrons and positrons were set as $m_p = 2m_e$. In both cases, the emission region was specified with a thickness of several cells of the computational grid. The voltage amplitude in the layers and the position of the emission boundary were calculated depending on the injected current for two different positions of the initial emission region. In the first case (*Emission region 1*), the emission region was set at the center of the computational region; in the second case (*Emission region 2*), it was shifted to the cathode to a position of a quarter of the gap.

Let's take a closer look at the layer formation mechanism. If the condition for volume emission is in the center and the thickness of this layer is much less than the width of the diode, then at the moment of charge accumulation in this region and the establishment of the Child-Langmuir current for both types of particles, the voltages between the layers will be divided in accordance with the following relationship:

$$I_c = \frac{4}{9}\varepsilon_0\sqrt{\frac{2e}{m_p}}\frac{S_c}{d_c^{\,2}}U_c^{\frac{3}{2}} = \frac{4}{9}\varepsilon_0\sqrt{\frac{2e}{m_e}}\frac{S_a}{d_a^{\,2}}U_a^{\frac{3}{2}} = I_a \qquad (6)$$

or

$$\left(\frac{m_e}{m_p}\right)^{\frac{1}{3}} U_c = U_a . \tag{7}$$

A similar relationship can be obtained for the emission region, which is located in an arbitrary place of the diode or has a certain longitudinal size. In the latter case, it will be necessary to take into account that the charge accumulation will occur within this region and the currents will differ from the values calculated by formula (1).

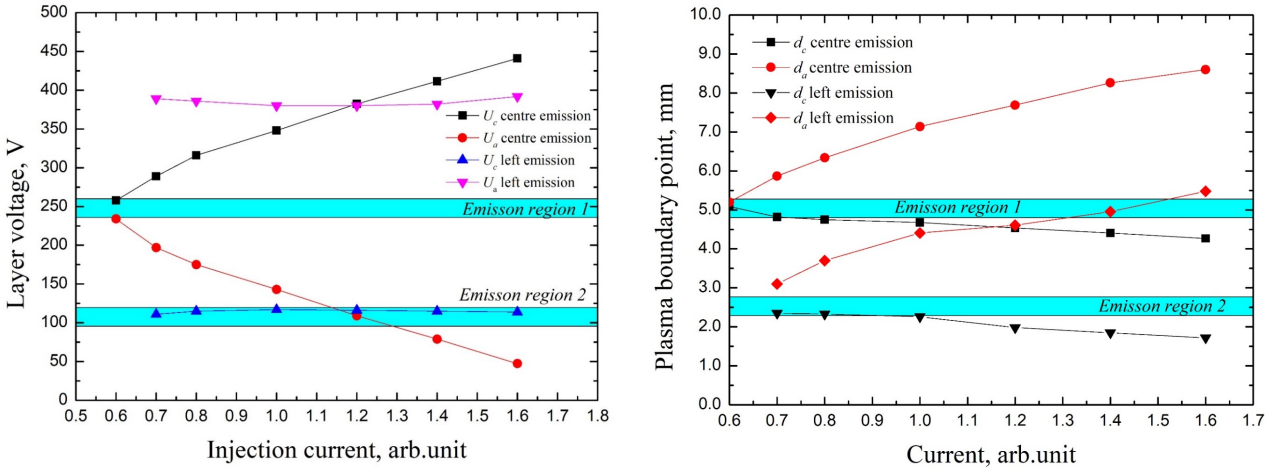

Fig.6. Voltage in the cathode and anode layers and the position of the plasma boundary for different emission currents and different emission plane position in the diode.

The conditions under which the voltage division occurs in accordance with the reasoning described above correspond to the points in Fig.6a and Fig.6b, which are located on the left side. Further, with an increase in the emission current, the behavior of the voltage and the width of the layers depending on the initial position of the emission boundary turns out to be different.

For the emission region, which was set in the center with an increase in the injection current, the position of the cathode layer practically remains unchanged (black and red curves), and the matching occurs due to a change in voltages. In the second case, due to the closer position of the electrode and the lower impedance, the voltages in the layers practically do not change with increasing current (blue and magenta curves). At the same time, the nature of the expansion of the "plasma" region remains practically unchanged.

Thus, depending on the initial impedance ratio in the layers, we get two different situations. In the first case, the voltages in the cathode and anode layers practically do not change with a change in the discharge current; in the other case, they change almost linearly. At this stage, it is still difficult to interpret the results of numerical simulation in relation to specific conditions of the auxiliary discharge. Under real conditions, when the current changes and, consequently, the voltage in the layers changes, the electron distribution function can also change. The scale of these changes will determine the condition for ionization in the discharge. Therefore, the assumptions that were used in the simulation require detailed verification, both from the modeling and experimental point of view. This will be the goal of our further research.

4. Conclusion

In this work, the region of the auxiliary discharge of an electron accelerator based on a non-self-sustaining high-voltage glow discharge was studied. Using a simple concept of an auxiliary

discharge as two Child-Langmuir diodes (flat and cylindrical) that are matched by a layer of conductive plasma, we can estimate the voltage range in the cathode and anode layers. For small currents, the estimate is in good agreement with previous experimental results. From a modeling standpoint, steps have been taken for a similar description. Different regimes of the behavior of the voltage in the layers and the behavior of the plasma boundary are obtained depending on the initial conditions. At this stage, only the first preliminary results have been obtained and work in this direction will be continued.

Acknowledgement

The work was carried out within the framework of the state assignment of the Ministry of Science and Higher Education of the Russian Federation on the topic FWRM-2021-0007, FWRM-2021-0014.

4. References

[1] Sokovnin S.Yu., *Nanosecond electron accelerators and radiation technologies based on them (Nanosekundnie uskoriteli i radiatsionnie tehnologii na ih osnove (in Russian))*. (Yekaterinburg: UrO RAS. 2007).
[2] Pushkarev A.I., Novoselov Yu.N., Remnev G.E., *Chain processes in low-temperature plasma (Tsepnie protsessi v nizkotemperaturnoy plasme (in Russian))*. (Novosibirsk: Science, 2006).
[3] Rostov V.V., et al., *The Siberian Medical Journal*, *(Sibirskiy meditsinskiy jurnal (in Russian)),* **27**(1), 141, 2012;
[4] Kryazhev Y.G., et al., *Tech. Phys. Lett.*, **42**, 981, 2016); doi: 10.1134/S1063785016100102
[5] Kosogorov S.L., et al., *Russ. Phys. J.*, **63**, 1686, 2021; doi: 10.1007/s11182-021-02222-8
[6] Kovivchak V.S., et al., *Vacuum*, **198**, 110885, 2022; doi: 10.1016/j.vacuum.2022.110885.
[7] Pigache D., Fournier G., *J. Vac. Sci. Technol.*, **12**(6), 1197, 1975; doi: 10.1116/1.568492
[8] Gurashvili V.A., et al., *Instruments and Experimental Techniques*, **63**(2), 227, 2020; doi: 10.1134/S0020441220030021
[9] Haijuan Mei, et al., *Surface & Coatings Technology*, **405**, 126514, 2020; doi: 10.1016/j.surfcoat.2020.126514
[10] Doroshkevich S.Yu., et al., *J. Phys.: Conf. Ser.*, **2064**, 012116, 2021; doi: 10.1088/1742-6596/2064/1/012116
[11] Doroshkevich S., Levanisov V., Lopatin I., Vorobyov M., Torba M., Kovalsky S., Sulakshin S., *8th Int. Cong. on Energy Fluxes and Radiation Effects (EFRE) – 22st Int. Symp. on High-Current Electronics, 2–8 October, Tomsk, Book of abstract*, 22, 2022; url: https://efre2022.hcei.tsc.ru/files/abstracts/S1-O-031103.pdf
[12] Doroshkevich S., et al., *Proc. of 7th Int. Cong. on Energy Fluxes and Radiation Effects (EFRE) – 21st Int. Symp. on High-Current Electronics*, Tomsk, 42, 2020; doi: 10.1109/EFRE47760.2020
[13] Langmuir I*., Phys. Rev.,* **2**, 450; 1913; doi: 10.1103/PhysRev.2.450
[14] Langmuir I., Blodgett K.B., *Phys. Rev.,* **22**, 347, 1923; doi: 10.1103/PhysRev.22.347
[15] Langmuir I., Blodgett K.B., *Phys. Rev.*, **24**, 49, 1924; doi: 10.1103/PhysRev.24.49
[16] Sysun V.I., Ignahin V.S., *J. Tech. Phys., [in Russian]*, **82**(7), 60, 2012; url: https://journals.ioffe.ru/articles/viewPDF/10650
[17] Grishkov A.A., Vorobyov M.S., Doroshkevich S.Yu., Shklyaev V.A., *Proc. of 8th Int. Cong. on Energy Fluxes and Radiation Effects, 2–8 October, Tomsk,* 2022; doi: 10.56761/EFRE2022.S1-P-049004
[18] Verboncoeur J.P., et al., *Comput. Phys. Commun.,* **87**, 199, 1995; doi: 10.1016/0010-4655(94)00173-Y